Taylor & Francis
Taylor & Francis Group

RESEARCH PAPER

OPEN ACCESS | Check for updates

Design, synthesis and biological evaluation of novel diarylpyridine derivatives as tubulin polymerisation inhibitors

Shanbo Yang[a,b], Chao Wang[a,b], Lingyu Shi[a,b], Jing Chang[a,b], Yujing Zhang[c], Jingsen Meng[a,b], Wenjing Liu[a,b], Jun Zeng[a,b], Renshuai Zhang[a,b], Yingchun Shao[a,b] and Dongming Xing[a,b,d]

[a]The Affiliated Hospital of Qingdao University, Cancer Institute, School of Basic Medicine, Qingdao University, Qingdao, China; [b]Qingdao Cancer Institute, Qingdao, China; [c]The Affiliated Cardiovascular Hospital of Qingdao University, Qingdao University, Qingdao, China; [d]School of Life Sciences, Tsinghua University, Beijing, China

ABSTRACT

A set of novel diarylpyridines as anti-tubulin agents were designed, synthesised using a rigid pyridine as a linker to fix the cis-orientation of ring-A and ring-B. All of the target compounds were evaluated for their in vitro antiproliferative activities. Among them, **10t** showed remarkable antiproliferative activities against three cancer cell lines (HeLa, MCF-7 and SGC-7901) in sub-micromolar concentrations. Consistent with its potent antiproliferative activity, **10t** also displayed potent anti-tubulin activity. Cellular mechanism investigation elucidated **10t** disrupted the cellular microtubule structure, arrested cell cycle at G2/M phase and induces apoptosis. Molecular modelling studies showed that **10t** could bind to the colchicine binding site on microtubules. These results provide motivation and further guidance for the development of new CA-4 analogues.

Introduction

Microtubules are hollow tubular structures composed of heterodimers of α-tubulin and β-tubulin, which have a variety of roles in eukaryotic cells, including maintenance of cell morphology, cell growth, cell motility, material transport, organelle transport, signalling, mitosis, etc.[1–3] If the dynamic cycle of microtubule assembly–disassembly is disrupted, the mitotic process of tumour cells is affected, thereby inhibiting their growth and leading to apoptosis.[4] Therefore, drugs that interfere with the kinetics of microtubule protein depolymerisation and polymerisation are an important class of antitumor drugs.[5] Several clinical agents have been developed (e.g. paclitaxel and vincristine), but there are currently no FDA-approved inhibitors of microtubulin at the colchicine site. The development of microtubulin polymerisation inhibitors targeting the colchicine binding site has, therefore, attracted the interest of many medicinal chemists.[6]

Combretastatin A-4 (**1**, Figure 1) is a natural product, first extracted from the bark of the South African willow tree Combretum caffrum in 1989, that inhibits tubulin polymerisation by interacting with colchicine binding site on tubulin.[7] This cis-stilbene shows excellent cytotoxicity against a wide range of human cancer cell lines, including multidrug-resistant cancer cell lines.[8,9] CA-4P (**2**, Figure 1), its soluble prodrug, is currently under clinical investigation as a combination therapy for various multidrug-resistant solid tumours.[10] Due to the structural simplicity of CA-4, numerous structure-activity relationships (SAR) studies have been performed on this compound and its analogs by many academic and industrial groups. SAR studies have shown that the cis-orientation of the double bond and the presence of 3,4,5-trimethoxyphenyl as ring A are essential to produce

potent potency.[11] A ring is an essential requirement for potent cytotoxicity. Unfortunately, CA-4 and other olefinic analogs are prone to isomerise to inactive trans-forms during storage and administration.[12] In order to avoid the stability problems of CA-4, the olefinic groups of the A and B rings are fixed by introducing various cyclic structures such as three, five and six-membered rings.[13–15]

Pyridine is a six-membered aromatic heterocycle containing a nitrogen atom, and its derivatives (**3–6**, Figure 1) have been of interest because of its ease of preparation and many potential pharmacological properties,[16] including anxiolytic,[17] anti-ulcer[18] and anti-tubulin activities.[19] For example, a series of substituted pyridine compounds have been reported as tubulin polymerisation inhibitors (**7–9**, Figure 1).[20–22]

In our study, pyridine fragment was introduced into the CA-4 skeleton to replace the olefinic group between the A and B rings. As a result, a series of diarylpyridines derivatives (**10**, Figure 2) were designed and synthesised. The newly synthesised target compounds were investigated for their biological activities to explore preliminary SAR and molecular modelling was performed to elucidate their possible binding modes in tubulin.

Results and discussion

Chemistry

The synthetics of target compounds **10a-10u** was shown in Scheme 1. Firstly, the 3-bromo-5-iodopyridine (**12**) was synthesised by using 3,5 dibromo-pyridine (**11**) as the starting material.[23] Subsequently, **12** reacted with 3,4,5-trimethoxybenzeneboronic

---

Figure 1. Chemical structures of CA-4, CA-4P, and some pyridine derivatives.
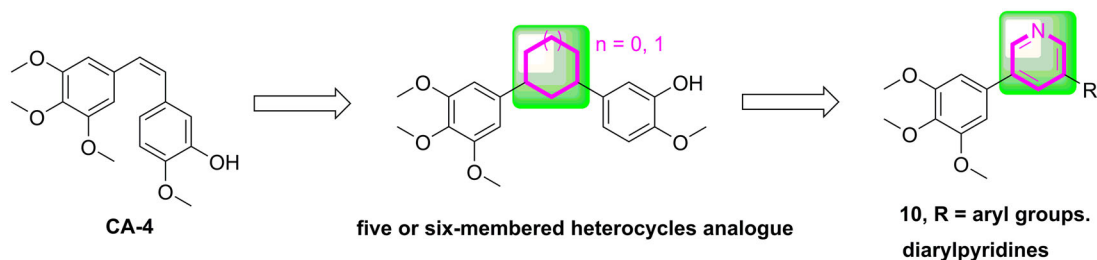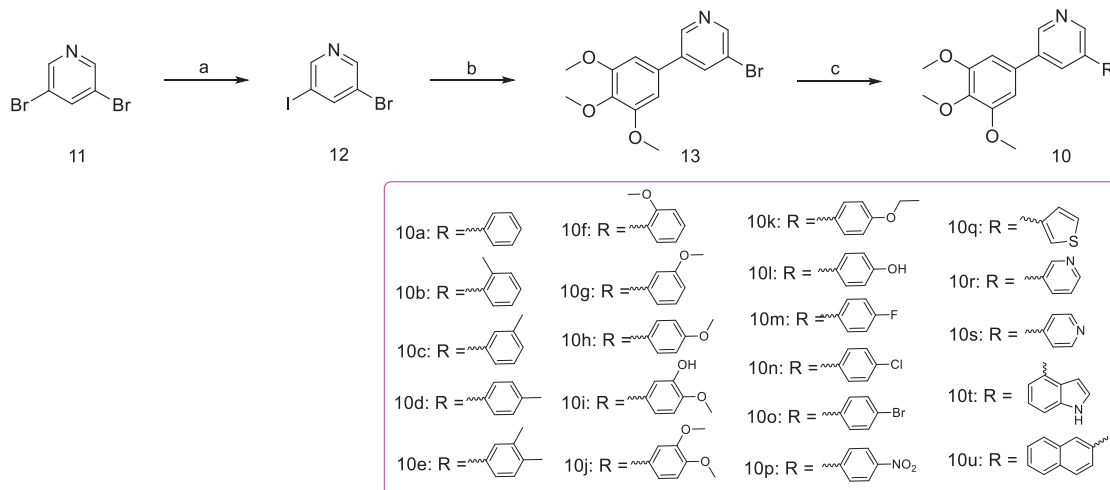

Figure 2. The rational design of target compounds.

Scheme 1. Reagents and conditions (a) *iPr*MgCl·LiCl, iodine, piperidine, THF, −10 to 5 °C, 10 min; (b) 3,4,5-trimethoxybenzeneboronic acid, Pd(PPh₃)₄, K₂CO₃, 1,4-dioxane/ H₂O = 3/1, N₂ atmosphere, 126 °C, M.W., 25 min; (c) substituted phenylboronic acid, Pd(PPh₃)₄, K₂CO₃, 1,4-dioxane/H₂O = 3/1, N₂ atmosphere, 126 °C, M.W., 25 min.

Table 1. Antiproliferative activity of all compounds.

Compounds	(IC$_{50}$ ± SD, μM)[a]		
	HeLa	SGC-7901	MCF-7
10a	20.21 ± 2.1	30.57 ± 2.5	39.83 ± 4.7
10b	50.62 ± 4.7	55.31 ± 5.6	>60
10c	3.28 ± 0.27	5.24 ± 0.69	8.49 ± 0.86
10d	15.22 ± 1.2	16.58 ± 2.2	13.94 ± 1.9
10e	>60	>60	>60
10f	37.83 ± 3.6	>60	25.80 ± 2.7
10g	17.78 ± 1.0	18.91 ± 0.97	>60
10h	4.20 ± 0.8	9.73 ± 1.7	8.54 ± 0.86
10i	13.74 ± 1.2	14.32 ± 1.1	19.58 ± 2.2
10j	>60	>60	>60
10k	39.63 ± 4.1	>60	>60
10l	18.81 ± 1.9	16.88 ± 1.7	29.61 ± 2.8
10m	>60	>60	>60
10n	30.83 ± 4.1	>60	>60
10o	>60	>60	>60
10p	>60	40.10 ± 5.2	>60
10q	>60	>60	>60
10r	55.21 ± 6.6	49.81 ± 5.1	>60
10s	>60	>60	>60
10t	**0.19 ± 0.013**	**0.30 ± 0.030**	**0.33 ± 0.028**
10u	>60	>60	>60
CA-4[b]	0.05 ± 0.004	0.08 ± 0.006	0.04 ± 0.002

Bold represents the IC$_{50}$ value of the target compound with the best activity.
[a]IC$_{50}$: the half maximal inhibitory concentration.
[b]Used as positive controls.

acid, Pd(PPh$_3$)$_4$ and K$_2$CO$_3$ in 1,4-dioxane/H$_2$O to afford 3-bromo-5–(3,4,5-trimethoxyphenyl)pyridine (**13**).[24] Lastly, **13** was reacted with the corresponding phenylboronic acid *via* Suzuki crosscoupling reaction to generate target compounds **10a-10u**.[25]

Biological evaluation

In vitro antiproliferative activity

The antiproliferative activities of diarylpyridines **10a-10u** were evaluated against human cancer cell lines, namely cervical (HeLa), gastric adenocarcinoma (SGC-7901) and breast (MCF-7), respectively, using the standard MTT assay with CA-4 as positive control. As illustrated in Table 1, some target compounds exhibited moderate to potent antiproliferative activities. Among them, **10t**, which contained an indole moiety as the B ring, displayed the most potent antiproliferative activities against HeLa, SGC-7901 and MCF-7 cell lines with IC$_{50}$ values of 0.19, 0.30 and 0.33 μM, respectively.

The SAR of the 21 target compounds have been summarised. Firstly, a sharply decline of antiproliferative activity was observed when other aryl groups such as thiophene (**10q**), pyridine (**10r** and **10s**) and naphthalene (**10u**) were introduced to replace the B ring. Furthermore, when the B ring is benzene, **10a** with the unsubstituted B ring displayed moderate active, the introduction of electron donating groups on B ring, such as -CH$_3$ (**10c**, **10d**), -OCH$_3$ (**10g**, **10h**), -OCH$_2$CH$_3$ (**10k**), −3-OH-4-OCH$_3$ (**10i**), resulted in maintenance or increase in antiproliferative activity. However, the antiproliferative activity was decreased when introduced electron withdrawing groups on B-ring, such as, -F (**10m**), -Cl (**10n**), -Br (**10o**) and -NO$_2$ (**10p**). Furthermore, the simultaneous introduction of -CH$_3$ (**10e**) and -OCH$_3$ (**10j**) at the 3,4-position of the B-ring resulted in drastically decreased inhibitory activity, probably due to two methoxy groups are bulky and have steric hindrance.
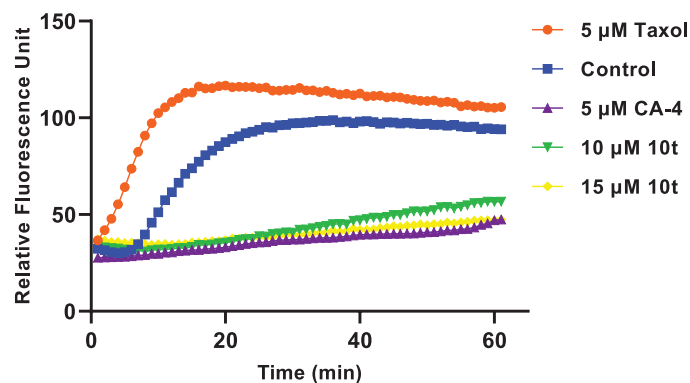

Figure 3. Effect of **10t** on tubulin polymerisation. Tubulin had been pre-incubated for 1 min with **10t** at 10 and 15 μM, CA-4 at 5 μM, taxol at 5 μM or vehicle DMSO at room temperature before GTP was added to start the tubulin polymerisation reactions. The reaction was monitored at 37 °C.

Tubulin polymerisation

CA-4 binds to microtubule heterodimers, thereby inhibiting microtubule polymerisation. In order to investigate whether the target compound **10t** act on the microtubule system, **10t** were selected and compared with the positive control drug CA-4 and the negative control drug taxol on the inhibition of tubulin polymerisation. As shown in Figure 3, **10t** significantly inhibited tubulin polymerisation compared with the negative control drug, taxol. **10t** inhibited tubulin polymerisation in a dose-dependent manner. The results showed that **10t** act on the tubulin system and interfere with tubulin polymerisation.

Analysis of immunofluorescence staining

Microtubule inhibitors can inhibit the formation of spindle filaments, lead to improper chromosome segregation, hinder the division process after metaphase, and which can have some effect on the cytoskeleton. To further determine the effect of target compound **10t** on tubulin, immunofluorescence experiments were used to observe the effects of 2-fold IC$_{50}$ **10t** and 2-fold IC$_{50}$ CA-4 on the microtubule network on Hela cells. As shown in Figure 4, untreated cells exhibited normal arrangement and organisation of microtubules. When treated with the **10t** and CA-4, microtubules became shorter and wrapped around the nucleus compared to the control group. The results showed that the **10t** exhibited similar characteristics to CA-4 and could disrupt the microtubule network and destabilise the microtubules.

Analysis of cell cycle

To assess the effect of target compounds on mitosis, the effect of **10t** on Hela cell cycle progression was next investigated by flow cytometry. In this study, Hela cells were treated with increasing doses of **10t** for 24 h. As shown in Figure 5, it was found that the **10t** inhibited the cells at 1-fold IC$_{50}$, 2-fold IC$_{50}$ and 3-fold IC$_{50}$, respectively. The proportions of cells blocked in G2/M phase were 26.02%, 40.22% and 87.87%, while the proportion of untreated control cells in G2/M phase was 11.75%. **10t** was demonstrated to clearly cause G2/M phase arrest in a time-dependent manner.

Analysis of cell apoptosis

Appearance of cell cycle arrest leads to apoptosis. To assess whether the target compounds can induce apoptosis, **10t** were detected on Hela cells using Annexin V-FITC/PI. As shown in Figure 6, it was found that the proportion of apoptotic cells in the
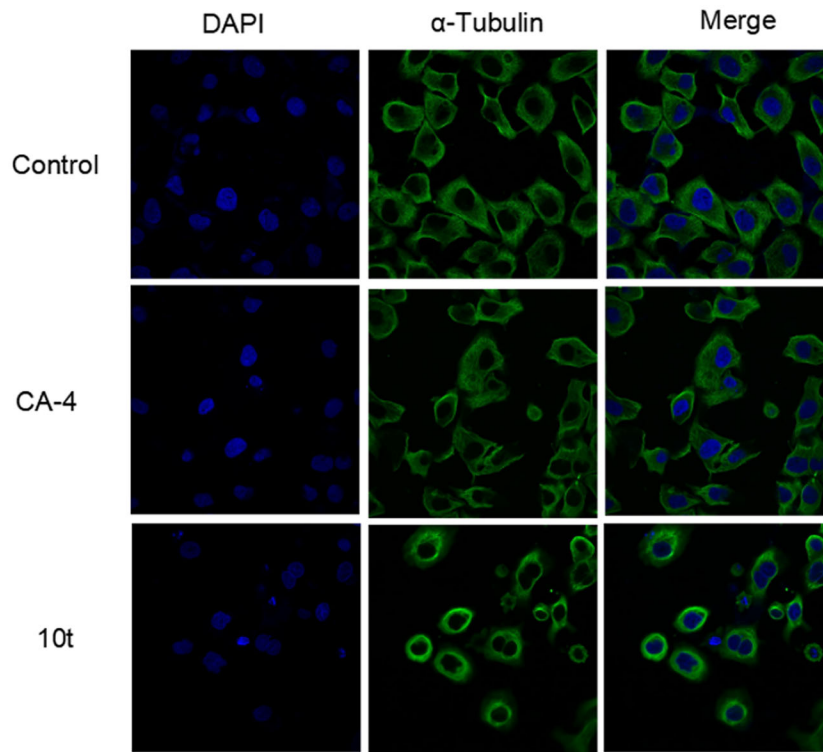
Figure 4. Effects of 2-fold IC$_{50}$ CA-4 and 2-fold IC$_{50}$ **10t** on the cellular microtubule networks of Hela cells by immunofluorescence assay. Microtubules and unassembled microtubule proteins stained with α-tubulin primary antibody and FITC secondary antibody, shown in green, and nuclei stained with DAPI, shown in the blue colour.

Figure 5. Cell cycle distribution of Hela cells after 24 h treatment with 1-fold IC$_{50}$, 2-fold IC$_{50}$ and 3-fold IC$_{50}$ of **10t**. (A) Control, (B) 1-fold IC$_{50}$, (C) 2-fold IC$_{50}$ and (D) 3-fold IC$_{50}$.

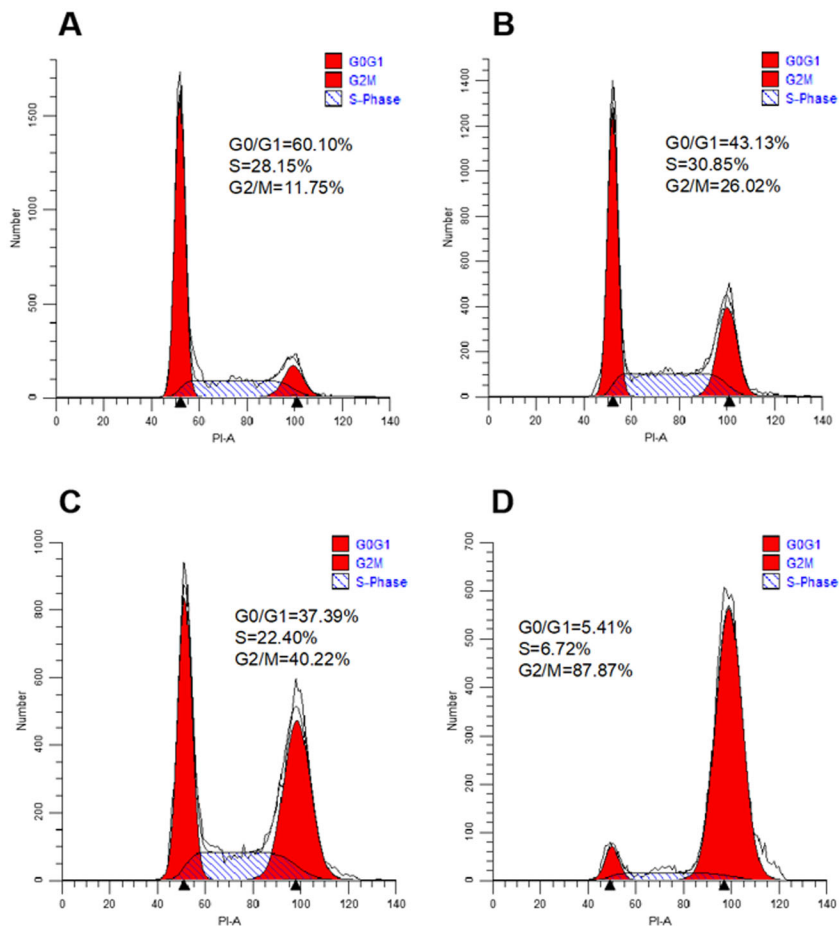**Figure 6.** Proportion of apoptotic cells in Hela cells after 48 h treatment with 1-fold IC_{50}, 2-fold IC_{50} and 3-fold IC_{50} of **10t**. (A) Control, (B) 1-fold IC_{50}, (C) 2-fold IC_{50} and (D) 3-fold IC_{50}.
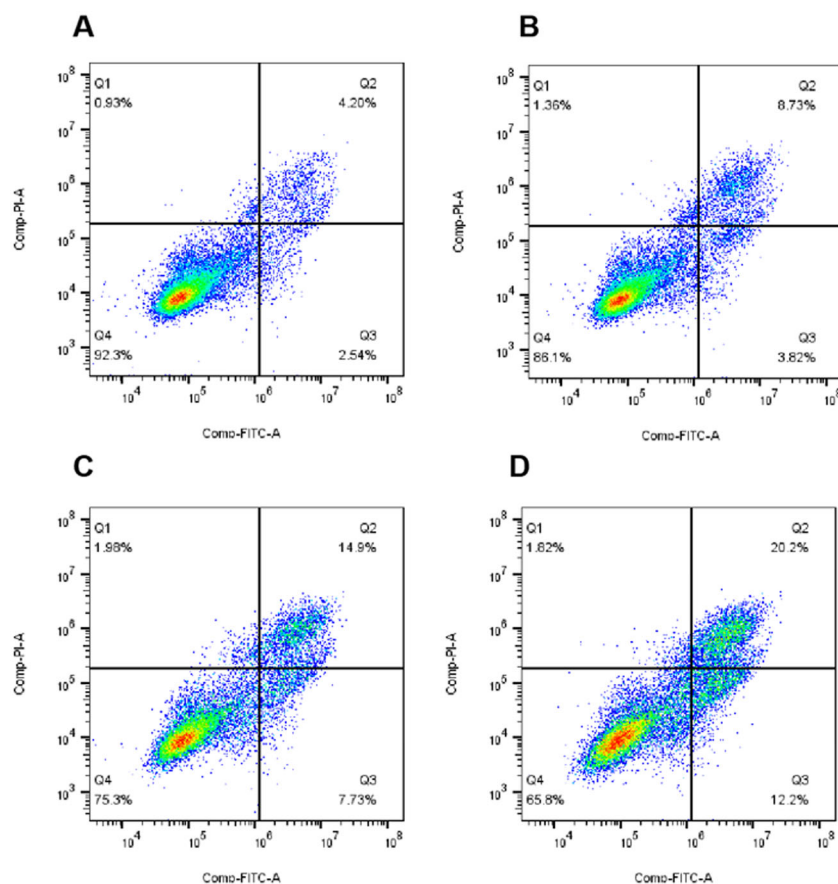
untreated control group was 7.67%. After treatment with 1-fold IC_{50}, 2-fold IC_{50} and 3-fold IC_{50}, the proportions of apoptotic cells were 13.91%, 24.61% and 34.22%. The results of apoptosis showed that **10t** induced Hela apoptosis in a dose-dependent manner.

Molecular modelling study

The representative compound **10t** was firstly selected to explain the reasons for the variability in the potency *via* molecular docking analysis with tubulin crystal structure (PDB: 1SA0) using the CDOCKER program of Discovery Studio 3.0 software. As given in Figure 7, the 3,4,5-trimethoxybenzoyl A ring of **10t** was located deeply into the β-subunit of tubulin. The B ring of **10t** extends towards the α/β-tubulin interface and several important amino acids of tubulin formed hydrogen bond interactions with **10t**. The residue of β-ASN249 forms a hydrogen bond with the oxygen of the methoxy group (A ring). Furthermore, nitrogen atom of pyridine forms a hydrogen bond with the residue β-SER178. The docking results suggested that **10t** may exhibit its biological activities by binding to colchicine site.

Conclusion

In summary, we replaced the double bond linker between the A and B rings by introducing a pyridine fragment into the CA-4 skeleton. We developed a series of diarylpyridines and evaluated their antiproliferative activity and tubulin polymerisation inhibition. Some synthesised compounds displayed moderate to potent antiproliferative activities with IC_{50} values at the sub-micromolar level. Among compounds, the existence of indole group was the main factor affecting the biological activity. **10t** has broad-spectrum antitumor activity against all tumour cell lines tested with IC_{50} value of 0.19–0.33 μM. Consistent with its antiproliferative activity, **10t** also exhibited potent antitubulin activity, similar to that of CA-4. Further mechanistic studies confirmed that **10t** was a microtubule-destabilizing agent that induced the accumulation of cells in the G2/M phase, caused cell mitotic catastrophe and apoptosis. Additionally, the results of docking study showed that **10t** may bind to colchicine binding site of tubulin. Our work not only expands the exploration of the linker modification of tubulin inhibitor CA-4 but also provides a set of rigid analogues with moderate to potent antiproliferative activity.

Experiment section

Chemistry

Materials and methods

All reagents and solvents were obtained from commercial sources. The reaction was monitored by TLC with silica gel plates under ultraviolet (UV) light (wavelength: 365 nm and 254 nm). ^1H (500 MHz) and ^{13}C NMR (125 MHz) were measured on an Agilent ProPulse 500 MHz at room temperature using $CDCl_3$ as solvent. High-resolution mass spectra (HRMS) were recorded by Agilent Accurate-Mass Q-TOF 6530 instrument in ESI mode. The microwave reactions were carried out in a single mode cavity microwave synthesiser (CEM Corporation, NC, USA).
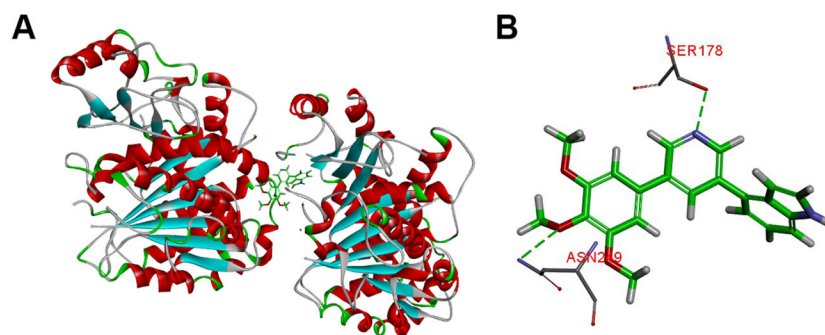
Figure 7. (A) The binding mode of compound **10t** in the colchicine binding site of tubulin; (B) overlay of **10t** in the binding site.

General synthetic procedures for 3-bromo-5-iodopyridine (12)

To a solution of 3,5dibromo-pyridine (5.4 mmol) in THF (25 ml), was added a solution of *iPr*MgCl.LiCl (5.9 mmol, 1.3 M in THF) at −10 °C. After 10 min of stirring a solution of iodine (5.9 mmol) in THF (10 ml) was added dropwise, keeping the temperature below −5 °C. After 10 min of stirring Et₂O (100 ml) was added and was washed with NaHSO₃ sat. (30 ml). Organic extract was washed with brine (50 ml), dried over Na_2SO_4, filtered and concentrated to give the desired product without further necessary purification.

General synthetic procedures for 3-bromo-5-(3,4,5-trimethoxyphenyl)pyridine (13)

A mixture of **12** (0.40 mmol), Pd(PPh₃)₄ (0.04 mmol), and K_2CO_3 (0.48 mmol), and 3,4,5-trimethoxybenzeneboronic acid (0.41 mmol) in 1,4-dioxane/H_2O (15 ml, 3:1) was degassed and purged with N_2 for about three times. After stirred at irradiated in a microwave reactor for 25 min at 130 °C (indicated by TLC) under N_2 atmosphere, the reaction mixture was poured into H_2O (50 ml) and extracted with ethyl acetate (80 ml × 3). The combined organics were washed with brine (10 ml × 3), dried over anhydrous Na_2SO_4, filtered and concentrated under vacuum to give a residue, which was purified by column 300 chromatography using a mixture of petroleum ether and ethyl acetate (3:1) as an eluent to provide the target compound **13** in yields of 80%.

General synthetic procedures for diarylpyridines (10)

A mixture of **13** (0.10 mmol), Pd(PPh₃)₄ (0.01 mmol), and K_2CO_3 (0.12 mmol), and substituted phenylboronic acid (0.11 mmol) in 1,4-dioxane/H_2O (5 ml, 3:1) was degassed and purged with N_2 for about three times. After stirred at irradiated in a microwave reactor for 25 min at 130 °C (indicated by TLC) under N_2 atmosphere, the reaction mixture was poured into H_2O (50 ml) and extracted with ethyl acetate (80 ml × 3). The combined organics were washed with brine (10 ml × 3), dried over anhydrous Na_2SO_4, filtered and concentrated under vacuum to give a residue, which was purified by column 300 chromatography using a mixture of petroleum ether and ethyl acetate (3:1) as an eluent to provide the target compounds (**10a-10u**) in yields of 42–95%.

3-Phenyl-5-(3,4,5-trimethoxyphenyl)pyridine (10a).

White solid; yield: 42%; m.p. 116–117 °C; ¹H NMR (500 MHz, CDCl₃) δ 8.89 (s, 2H), 8.09 (s, 1H), 7.64 (d, J = 7.3 Hz, 2H), 7.53 (t, J = 7.5 Hz, 2H), 7.47 (t, J = 7.3 Hz, 1H), 6.80 (s, 2H), 3.94 (s, 6H), 3.92 (s, 3H); ¹³C NMR (125 MHz, CDCl₃) δ 153.89 (2C), 144.93 (2C), 138.64, 134.11, 133.64 (2C), 129.67, 129.28 (2C), 128.69, 127.56, 127.30 (2C), 104.62 (2C), 61.00, 56.32 (2C); HRMS calcd for $C_{20}H_{20}NO_3$ [M + H]⁺ 322.1443, found 322.1439.

3-(O-Tolyl)-5-(3,4,5-trimethoxyphenyl)pyridine (10b).

White solid; yield: 89%; m.p. 84–86 °C; ¹H NMR (500 MHz, CDCl₃) δ 8.83 (s, 1H), 8.59 (s, 1H), 7.84 (s, 1H), 7.36–7.32 (m, 2H), 7.32–7.27 (m, 2H), 6.80 (s, 2H), 3.93 (s, 6H), 3.91 (s, 3H), 2.32 (s, 3H); ¹³C NMR (125 MHz, CDCl₃) δ 153.82 (2C), 148.01, 145.97, 138.46, 137.70, 135.65, 135.16, 133.21, 130.68 (2C), 129.89, 128.37, 126.19, 124.82, 104.50 (2C), 60.98, 56.28 (2C), 20.42; HRMS calcd for $C_{21}H_{22}NO_3$ [M + H]⁺ 336.1600, found 336.1604.

3-(M-Tolyl)-5-(3,4,5-trimethoxyphenyl)pyridine (10c).

White solid; yield: 74%; m.p. 80–81 °C; ¹H NMR (500 MHz, CDCl₃) δ 8.83 (s, 2H), 7.99 (s, 1H), 7.44 (d, J = 7.0 Hz, 2H), 7.40 (t, J = 7.9 Hz, 1H), 7.26 (d, J = 5.6 Hz, 1H), 6.81 (s, 2H), 3.95 (s, 6H), 3.91 (s, 3H), 2.46 (s, 3H); ¹³C NMR (125 MHz, CDCl₃) δ 153.78 (2C), 146.88, 146.68, 138.87 (2C), 138.39, 137.69, 133.65, 132.86, 129.05 (2C), 128.02, 124.40, 109.99, 104.64 (2C), 60.98, 56.32 (2C), 21.52; HRMS calcd for $C_{21}H_{22}NO_3$ [M + H]⁺ 336.1600, found 336.1601.

3-(P-Tolyl)-5-(3,4,5-trimethoxyphenyl)pyridine (10d).

White solid; yield: 55%; m.p. 152–153 °C; ¹H NMR (500 MHz, CDCl₃) δ 8.80 (s, 2H), 7.99 (s, 1H), 7.54 (d, J = 8.1 Hz, 2H), 7.32 (d, J = 7.9 Hz, 2H), 6.80 (s, 2H), 3.95 (s, 6H), 3.91 (s, 3H), 2.43 (s, 3H); ¹³C NMR (125 MHz, CDCl₃) δ 153.78 (2C), 146.57, 146.34, 138.39, 138.33 (2C), 134.70, 133.59, 132.78 (2C), 129.87 (2C), 127.10 (2C), 104.61 (2C), 60.98, 56.31 (2C), 21.17; HRMS calcd for $C_{21}H_{22}NO_3$ [M + H]⁺ 336.1600, found 336.1597.

3-(3,4-Dimethylphenyl)-5-(3,4,5-trimethoxyphenyl)pyridine (10e).

White solid; yield: 80%; m.p. 124–125 °C; ¹H NMR (500 MHz, CDCl₃) δ 8.79 (d, J = 18.9 Hz, 2H), 7.98 (t, J = 2.0 Hz, 1H), 7.41 (s, 1H), 7.38 (d, J = 7.7 Hz, 1H), 7.27 (d, J = 7.8 Hz, 1H), 6.80 (s, 2H), 3.95 (s, 6H), 3.91 (s, 3H), 2.37 (s, 3H), 2.34 (s, 3H); ¹³C NMR (125 MHz, CDCl₃) δ 153.77 (2C), 146.59, 146.24, 138.38, 137.47, 137.00, 136.89, 136.80, 135.13, 133.63, 132.84, 130.42, 128.44, 124.62, 104.63 (2C), 60.98, 56.31 (2C), 19.92, 19.50; HRMS calcd for $C_{22}H_{24}NO_3$ [M + H]⁺ 350.1756, found 350.1753.

3-(2-Methoxyphenyl)-5-(3,4,5-trimethoxyphenyl)pyridine (10f).

White solid; yield: 75%; m.p. 78–80 °C; ¹H NMR (500 MHz, CDCl₃) δ 8.75 (s, 2H), 8.00 (s, 1H), 7.44–7.33 (m, 2H), 7.09 (t, J = 7.5 Hz, 1H), 7.04 (d, J = 8.2 Hz, 1H), 6.80 (s, 2H), 3.94 (s, 6H), 3.91 (s, 3H), 3.84 (s, 3H); ¹³C NMR (125 MHz, CDCl₃) δ 156.61, 153.72 (2C), 148.85, 146.18, 138.22, 135.27, 133.80, 130.70 (2C), 129.76, 126.80, 121.10 (2C), 111.32, 104.60 (2C), 60.97, 56.26 (2C), 55.57; HRMS calcd for $C_{21}H_{22}NO_4$ [M + H]⁺ 352.1549, found 352.1547.

3-(3-Methoxyphenyl)-5-(3,4,5-trimethoxyphenyl)pyridine (10g).

White solid; yield: 43%; m.p. 94–96 °C; ¹H NMR (500 MHz, CDCl₃) δ

8.75 (s, 2H), 7.99 (s, 1H), 7.40 (td, $J = 9.4$, 1.6 Hz, 2H), 7.09 (t, $J = 7.5$ Hz, 1H), 7.04 (d, $J = 8.2$ Hz, 1H), 6.80 (s, 2H), 3.94 (s, 6H), 3.91 (s, 3H), 3.85 (s, 3H); ^{13}C NMR (125 MHz, CDCl$_3$) δ 156.61, 153.71 (2C), 148.95, 146.28, 138.20, 136.16, 135.22, 134.12, 133.84, 130.70, 129.73, 126.83, 121.10, 111.32, 104.59 (2C), 60.97, 56.26 (2C), 55.57; HRMS calcd for C$_{21}$H$_{22}$NO$_4$ [M + H]$^+$ 352.1549, found 352.1557.

3-(4-Methoxyphenyl)-5-(3,4,5-trimethoxyphenyl)pyridine (10h).
White solid; yield: 95%; m.p. 120–121 °C; ^{1}H NMR (500 MHz, CDCl$_3$) δ 8.76 (d, $J = 19.9$ Hz, 2H), 7.95 (s, 1H), 7.58 (d, $J = 8.7$ Hz, 2H), 7.04 (d, $J = 8.7$ Hz, 2H), 6.80 (s, 2H), 3.94 (s, 6H), 3.91 (s, 3H), 3.87 (s, 3H); ^{13}C NMR (125 MHz, CDCl$_3$) δ 159.92, 153.76 (2C), 146.58, 146.24, 138.35, 136.81, 136.26, 133.68, 132.38, 130.02, 128.35 (2C), 114.62 (2C), 104.60 (2C), 60.98, 56.30 (2C), 55.40; HRMS calcd for C$_{21}$H$_{22}$NO$_4$ [M + H]$^+$ 352.1549, found 352.1555.

2-Methoxy-5-(5-(3,4,5-trimethoxyphenyl)pyridin-3-yl)phenol (10i).
White solid; yield: 95%; m.p. 170–171 °C; ^{1}H NMR (500 MHz, CDCl$_3$) δ 8.76 (d, $J = 21.9$ Hz, 2H), 7.96 (s, 1H), 7.27 (d, $J = 2.2$ Hz, 1H), 7.13 (dd, $J = 8.3$, 2.2 Hz, 1H), 6.97 (d, $J = 8.3$ Hz, 1H), 6.79 (s, 2H), 3.93 (s, 9H), 3.90 (s, 3H); ^{13}C NMR (125 MHz, CDCl$_3$) δ 153.77 (2C), 147.39, 146.59, 146.31, 146.03, 138.37, 136.87, 136.43, 132.01, 128.54, 128.45, 118.74, 113.71, 111.40, 104.54 (2C), 60.97, 56.30 (2C), 56.04; HRMS calcd for C$_{21}$H$_{22}$NO$_5$ [M + H]$^+$ 368.1498, found 368.1498.

3-(3,4-Dimethoxyphenyl)-5-(3,4,5-trimethoxyphenyl)pyridine (10j).
White solid; yield: 81%; m.p. 110–112 °C; ^{1}H NMR (500 MHz, CDCl$_3$) δ 8.76 (d, $J = 17.0$ Hz, 2H), 7.94 (s, 1H), 7.19 (dd, $J = 8.3$, 2.1 Hz, 1H), 7.12 (d, $J = 2.1$ Hz, 1H), 7.00 (d, $J = 8.3$ Hz, 1H), 6.80 (s, 2H), 3.96 (s, 3H), 3.94 (s, 9H), 3.91 (s, 3H); ^{13}C NMR (125 MHz, CDCl$_3$) δ 153.78 (2C), 149.53, 149.45, 146.75, 146.46, 138.39, 136.86, 136.52, 133.67, 132.53, 130.51, 119.78, 111.74, 110.45, 104.67 (2C), 60.98, 56.33 (2C), 56.10, 56.04; HRMS calcd for C$_{22}$H$_{24}$NO$_5$ [M + H]$^+$ 382.1654, found 382.1657.

3-(4-Ethoxyphenyl)-5-(3,4,5-trimethoxyphenyl)pyridine (10k).
White solid; yield: 65%; m.p. 118–120 °C; ^{1}H NMR (500 MHz, CDCl$_3$) δ 8.76 (d, $J = 22.4$ Hz, 2H), 7.95 (s, 1H), 7.57 (d, $J = 8.7$ Hz, 2H), 7.03 (d, $J = 8.7$ Hz, 2H), 6.80 (s, 2H), 4.10 (q, $J = 7.0$ Hz, 2H), 3.95 (s, 6H), 3.91 (s, 3H), 1.46 (t, $J = 7.0$ Hz, 3H); ^{13}C NMR (125 MHz, CDCl$_3$) δ 159.29, 153.76 (2C), 146.59, 146.20, 138.34, 136.29, 133.72, 132.34 (2C), 129.84, 128.32 (2C), 115.15 (2C), 104.60 (2C), 63.61, 60.98, 56.31 (2C), 14.80; HRMS calcd for C$_{22}$H$_{24}$NO$_4$ [M + H]$^+$ 366.1705, found 366.1705.

4-(5-(3,4,5-Trimethoxyphenyl)pyridin-3-yl)phenol (10l).
White solid; yield: 57%; m.p. 211–212 °C; ^{1}H NMR (500 MHz, CDCl$_3$) δ 8.74 (d, $J = 22.3$ Hz, 2H), 7.97 (s, 1H), 7.55 (d, $J = 7.5$ Hz, 2H), 7.04 (d, $J = 8.5$ Hz, 2H), 6.80 (s, 2H), 3.95 (s, 6H), 3.91 (s, 3H); ^{13}C NMR (125 MHz, CDCl$_3$) δ 157.48, 153.77 (2C), 146.16, 145.62, 138.37, 133.60, 132.12 (2C), 132.02, 128.59 (2C), 128.40, 116.35 (2C), 104.59 (2C), 60.99, 56.32 (2C); HRMS calcd for C$_{20}$H$_{20}$NO$_4$ [M + H]$^+$ 338.1392, found 338.1394.

3-(4-Fluorophenyl)-5-(3,4,5-trimethoxyphenyl)pyridine (10m).
White solid; yield: 76%; m.p. 109–110 °C; ^{1}H NMR (500 MHz, CDCl$_3$) δ 8.78 (d, $J = 6.6$ Hz, 2H), 7.95 (s, 1H), 7.60 (dd, $J = 8.8$, 5.2 Hz, 2H), 7.20 (t, $J = 8.6$ Hz, 2H), 6.80 (s, 2H), 3.95 (s, 6H), 3.91 (s, 3H); ^{13}C NMR (125 MHz, CDCl$_3$) δ 163.01 (d, $J = 248.2$ Hz, 1C), 153.80 (2C), 146.94, 146.77, 138.46, 136.90, 135.72, 133.82, 133.44, 132.66, 128.96 (d, $J = 8.2$ Hz, 2C), 116.14 (d, $J = 21.6$ Hz, 2C), 104.63 (2C), 60.98, 56.32

(2C); HRMS calcd for C$_{20}$H$_{19}$FNO$_3$ [M + H]$^+$ 340.1349, found 340.1346.

3-(4-Chlorophenyl)-5-(3,4,5-trimethoxyphenyl)pyridine (10n).
White solid; yield: 63%; m.p. 136–137 °C; ^{1}H NMR (500 MHz, CDCl$_3$) δ 8.79 (d, $J = 9.0$ Hz, 2H), 7.95 (s, 1H), 7.57 (d, $J = 8.4$ Hz, 2H), 7.48 (d, $J = 8.5$ Hz, 2H), 6.80 (s, 2H), 3.95 (s, 6H), 3.91 (s, 3H); ^{13}C NMR (125 MHz, CDCl$_3$) δ 153.82 (2C), 147.21, 146.71, 138.50, 136.97, 136.13, 135.49, 134.58, 133.36, 132.65, 129.35 (2C), 128.52 (2C), 104.64 (2C), 60.99, 56.33 (2C); HRMS calcd for C$_{20}$H$_{19}$ClNO$_3$ [M + H]$^+$ 356.1053, found 356.1050.

3-(4-Bromophenyl)-5-(3,4,5-trimethoxyphenyl)pyridine (10o).
White solid; yield: 51%; m.p. 137–138 °C; ^{1}H NMR (500 MHz, CDCl$_3$) δ 8.82 (s, 2H), 8.02 (s, 1H), 7.53 (d, $J = 3.2$ Hz, 2H), 7.50 (d, $J = 2.0$ Hz, 2H), 7.26 (s, 2H), 3.96 (s, 6H), 3.92 (s, 3H); ^{13}C NMR (125 MHz, CDCl$_3$) δ 153.81 (2C), 146.58, 146.52, 138.47, 137.57, 136.57, 136.38, 133.42, 133.11, 132.44, 129.17 (2C), 127.29 (2C), 104.61 (2C), 60.99, 56.32 (2C); HRMS calcd for C$_{20}$H$_{19}$BrNO$_3$ [M + H]$^+$ 400.0548, found 400.0545.

3-(4-Nitrophenyl)-5-(3,4,5-trimethoxyphenyl)pyridine (10p).
Yellow solid; yield: 68%; m.p. 175–177 °C; ^{1}H NMR (500 MHz, CDCl$_3$) δ 8.87 (s, 2H), 8.36 (d, $J = 8.9$ Hz, 2H), 8.02 (s, 1H), 7.81 (d, $J = 8.9$ Hz, 2H), 6.80 (s, 2H), 3.95 (s, 6H), 3.91 (s, 3H); ^{13}C NMR (125 MHz, CDCl$_3$) δ 153.89 (2C), 148.39, 147.75, 146.83, 144.13, 138.70, 137.28, 134.46, 132.93 (2C), 128.10 (2C), 124.39 (2C), 104.68 (2C), 61.00, 56.36 (2C); HRMS calcd for C$_{20}$H$_{19}$N$_2$O$_5$ [M + H]$^+$ 367.1294, found 367.1291.

3-(Thiophen-3-yl)-5-(3,4,5-trimethoxyphenyl)pyridine (10q).
Yellow solid; yield: 90%; m.p. 145–147 °C; ^{1}H NMR (500 MHz, CDCl$_3$) δ 8.87 (s, 1H), 8.78 (s, 1H), 8.02 (t, $J = 1.9$ Hz, 1H), 7.60 (dd, $J = 2.9$, 1.3 Hz, 1H), 7.49 (dd, $J = 5.0$, 2.9 Hz, 1H), 7.44 (dd, $J = 5.0$, 1.3 Hz, 1H), 6.78 (s, 2H), 3.94 (s, 6H), 3.91 (s, 3H); ^{13}C NMR (125 MHz, CDCl$_3$) δ 153.83 (2C), 145.77, 145.42, 138.56, 138.31, 133.19, 132.55, 131.86, 127.27, 125.98, 124.90, 122.06, 104.63 (2C), 60.99, 56.33 (2C); HRMS calcd for C$_{18}$H$_{18}$NO$_3$S [M + H]$^+$ 328.1007, found 328.1004.

5-(3,4,5-Trimethoxyphenyl)-3,3'-bipyridine (10r).
White solid; yield: 62%; m.p. 160–161 °C; ^{1}H NMR (500 MHz, CDCl$_3$) δ 8.86 (dd, $J = 10.9$, 2.1 Hz, 2H), 8.74 (d, $J = 5.7$ Hz, 2H), 8.02 (t, $J = 2.2$ Hz, 1H), 7.57 (d, $J = 4.5$ Hz, 2H), 6.79 (s, 2H), 3.95 (s, 6H), 3.91 (s, 3H); ^{13}C NMR (125 MHz, CDCl$_3$) δ 153.88, 150.57 (2C), 148.61 (2C), 146.69, 145.14, 138.65, 137.20, 133.81, 133.00, 132.66 (2C), 121.70, 104.66 (2C), 60.99, 56.35 (2C); HRMS calcd for C$_{19}$H$_{19}$N$_2$O$_3$ [M + H]$^+$ 323.1396, found 323.1395.

5-(3,4,5-Trimethoxyphenyl)-3,4'-bipyridine (10s).
White solid; yield: 80%; m.p. 94–95 °C; ^{1}H NMR (500 MHz, CDCl$_3$) δ 8.91 (s, 1H), 8.84 (s, 1H), 8.80 (s, 1H), 8.69 (d, $J = 4.0$ Hz, 1H), 7.99 (s, 1H), 7.94 (d, $J = 7.9$ Hz, 1H), 7.44 (dd, $J = 7.8$, 4.9 Hz, 1H), 6.80 (s, 2H), 3.94 (s, 6H), 3.91 (s, 3H); ^{13}C NMR (125 MHz, CDCl$_3$) δ 153.85 (2C), 149.47, 148.30, 147.77, 146.77, 138.58, 137.11, 134.55, 133.47, 133.43, 133.11, 132.78, 123.81, 104.62 (2C), 60.99, 56.33 (2C); HRMS calcd for C$_{19}$H$_{19}$N$_2$O$_3$ [M + H]$^+$ 323.1396, found 323.1393.

4-(5-(3,4,5-Trimethoxyphenyl)pyridin-3-yl)-1H-indole (10t).
White solid; yield: 51%; m.p. 209–210 °C; ^{1}H NMR (500 MHz, CDCl$_3$) δ 8.95 (s, 1H), 8.83 (d, $J = 7.5$ Hz, 2H), 8.17 (s, 1H), 7.50 (d, $J = 8.1$ Hz, 1H), 7.37–7.30 (m, 2H), 7.29–7.23 (m, 1H), 6.85 (s, 2H), 6.73 (s, 1H), 3.95 (s, 6H), 3.93 (s, 3H); ^{13}C NMR (125 MHz, CDCl$_3$) δ 153.77 (2C), 148.16, 146.33, 138.28, 136.92, 136.76, 136.34, 134.40, 133.75,

130.34, 126.19, 125.29, 122.37, 119.98, 111.35, 104.60 (2C), 101.37, 61.00, 56.29 (2C); HRMS calcd for $C_{22}H_{21}N_2O_3$ [M + H]$^+$ 361.1552, found 361.1550.

3-(Naphthalen-2-yl)-5-(3,4,5-trimethoxyphenyl)pyridine (10u).

White solid; yield: 76%; m.p. 145–147 °C; ^{1}H NMR (500 MHz, CDCl$_3$) δ 8.95 (s, 1H), 8.82 (s, 1H), 8.11 (d, $J = 7.5$ Hz, 2H), 7.99 (d, $J = 8.5$ Hz, 1H), 7.94 (d, $J = 9.0$ Hz, 1H), 7.90 (d, $J = 9.0$ Hz, 1H), 7.77 (d, $J = 10.2$ Hz, 1H), 7.58–7.50 (m, 2H), 6.84 (s, 2H), 3.96 (s, 6H), 3.93 (s, 3H); ^{13}C NMR (125 MHz, CDCl$_3$) δ 153.81 (2C), 147.21, 146.95, 138.44, 136.95, 136.60, 134.98, 133.61, 133.57, 133.05, 132.95, 128.97, 128.22, 127.74, 126.70, 126.56, 126.33, 125.07, 104.68 (2C), 61.00, 56.35 (2C); HRMS calcd for $C_{24}H_{22}NO_3$ [M + H]$^+$ 372.1600, found 372.1598.

Biology experiment

MTT assay

The *in vitro* antiproliferative activity of the target compounds and CA-4 was measured by a standard MTT (meilunbio®, China) assay. Cervical cancer (HeLa), gastric adenocarcinoma (SGC-7901) and breast cancer (MCF-7) were used, respectively. Cells were inoculated in 96-well plates at a density of 2×10^3/well. After 24 h, the target concentration of drug was added to each well and incubated for 72 h at 37 °C under 5% CO$_2$. 20 μL of fresh medium containing 5 mg/ml MTT solution was added and incubation continued for 4 h. After removing the medium containing MTT from each well, 150 μL of dimethyl sulfoxide (DMSO) was added to each well until the purple formazan crystals was completely dissolved, placed in a multimode plate reader Victor Nivo 3S (Perkinelmer, USA) and the absorbance was measured at 490 nm.[26]

Tubulin polymerisation assay

The microtubule polymerisation ability of 10 and 15 μM **10t** was tested *in vitro* using the Microtubulin Kit (Cytoskeleton-Cat. #BK011P) by suspending microtubulin in ice-cold G-PEM buffer (80 mM PIPES, 2 mM MgCl$_2$, 0.5 mM EGTA, 1 mM GTP, 20% (v/v) glycerol) and adding to 96-well plates provided by the kit. **10t** were compared with the positive control drug 5 μM CA-4 and the negative control drug 5 μM taxol. The polymerisation of microtubule proteins was monitored at 1 min intervals (emission wavelength: 450 nm, excitation wavelength: 360 nm) for 61 min at 37 °C using a microplate reader (Tecan, Austria) and the absorbance values were used for calculation.[11,27]

Immunofluorescence assay

HeLa cells were inoculated in 6-well plates at a density of 2×10^5 per well and grown for 24 h. Cells were treated with 2-fold IC$_{50}$ of positive drugs CA-4 or the 2-fold IC$_{50}$ target compound for 24 h. Control and treated cells were washed in PBS, fixed in 4% paraformaldehyde solution for 20 min, then washed three times in PBST and permeabilised with 0.5% (v/v) Triton X-100 in PBS for 10 min. Cells were then closed with 3% bovine serum albumin (BSA) for 60 min. The α-microtubulin antibody (Abclonal, China) was diluted with 3% BSA (1:100) and incubated for 3 h. Cells were washed three times with PBST for 10 min each time to remove unbound primary antibody, then FITC-conjugated antimouse secondary antibody (1:100) and DAPI (1:100) were diluted with 3% BSA and incubated for a further 1 h. Cells were washed three times with PBST for 10 min each time to remove unbound secondary antibody and DAPI, and then immunofluorescence was detected by fluorescence confocal microscopy (Nikon, Japan).[28,29]

Cell cycle analysis

HeLa cells were inoculated in 6-well plates at a density of 2×10^5 per well and grown for 24 h. Cells were treated with 1-fold IC$_{50}$, 2-fold IC$_{50}$ and 3-fold IC$_{50}$ **10t** for 24 h. Cells were collected by centrifugation, washed with PBS and fixed overnight in ice-cold 70% ethanol. The fixed cells were collected by centrifugation and 100 μL of ribonuclease (RNase) was added. After a water bath at 37 °C for 30 min, 400 μL PI staining was added and the samples were stained for 30 min in the dark at 4 °C. Finally, the samples were analysed by flow cytometry (Beckman Coulter, USA). The data were processed and evaluated using software.[30,31]

Cell apoptosis analysis

HeLa cells were inoculated in 6-well plates at a density of 2×10^5 per well and grown for 24 h. Cells were treated with 1-fold IC$_{50}$, 2-fold IC$_{50}$ and 3-fold IC$_{50}$ **10t** for 48 h. After collecting the cells with trypsin without EDTA, the cells were washed twice with pre-cooled PBS, and Binding Buffer was added to the cell pellet to resuspend the cells. The concentration reached 1×10^6/ml, then stained with 5 μL Annexin-V FITC and 5 μL PI for 15 min in the dark, and measured by flow cytometry (Beckman Coulter, USA).[32,33]

Molecular modelling

Molecular modelling studies were performed using the CDOCKER program of the Discovery Studio 3.0 software, and the crystal structure of the tubulin complex (PDB: 1SA0) was retrieved from the RCSB protein database (http://www.rcsb.org/pdb). Hydrogen atoms are added to the crystal after the ligand is extracted. Charges are added to biopolymers via the CHARMm force field. Finally, **10t** was docked to the colchicine site of tubulin using the CDOCKER protocol.[34]

Disclosure statement

No potential conflict of interest was reported by the author(s).

Funding

References

1. Giodini A, Kallio MJ, Wall NR, Gorbsky GJ, Tognin S, Marchisio PC, Symons M, Altieri DC. Regulation of microtubule stability and mitotic progression by survivin. Cancer Res. 2002;62(9):2462–2467.
2. Lu Y, Chen J, Xiao M, Li W, Miller DD. An overview of tubulin inhibitors that interact with the colchicine binding site. Pharm Res. 2012;29(11):2943–2971.

3. Risinger AL, Giles FJ, Mooberry SL. Microtubule dynamics as a target in oncology. Cancer Treat Rev. 2009;35(3):255–261.

4. Wang C, Zhang Y, Xing D. Emerging tubulin inhibitors: a new hope for fungicides. J Agric Food Chem. 2021;69(38): 11151–11153.

5. Wang C, Zhang Y, Wu Y, Xing D. Developments of CRBN-based PROTACs as potential therapeutic agents. Eur J Med Chem. 2021;225:113749.

6. Steinmetz MO, Prota AE. Microtubule-targeting agents: strategies to hijack the cytoskeleton. Trends Cell Biol. 2018; 28(10):776–792.

7. Pettit GR, Singh SB, Hamel E, Lin CM, Alberts DS, Garcia-Kendall D. Isolation and structure of the strong cell growth and tubulin inhibitor combretastatin A-4. Experientia. 1989; 45(2):209–211.

8. Pettit GR, Minardi MD, Rosenberg HJ, Hamel E, Bibby MC, Martin SW, Jung MK, Pettit RK, Cuthbertson TJ, Chapuis JC. Antineoplastic agents. 509: synthesis of fluorcombstatin phosphate and related 3-halostilbenes(1). J Nat Prod. 2005; 68(10):1450–1458.

9. Pettit GR, Anderson CR, Herald DL, Jung MK, Lee DJ, Hamel E, Pettit RK. Antineoplastic agents. 487. Synthesis and biological evaluation of the antineoplastic agent 3,4-methylenedioxy-5,4'-dimethoxy-3'-amino-Z-stilbene and derived amino acid amides. J Med Chem. 2003;46(4):525–531.

10. Cushman M, Nagarathnam D, Gopal D, Chakraborti AK, Lin CM, Hamel E. Synthesis and evaluation of stilbene and dihydrostilbene derivatives as potential anticancer agents that inhibit tubulin polymerization. J Med Chem. 1991;34(8): 2579–2588.

11. Liu R, Huang M, Zhang S, Li L, Li M, Sun J, Wu L, Guan Q, Zhang W. Design, synthesis and bioevaluation of 6-aryl-1-(3,4,5-trimethoxyphenyl)-1H-benzo[d]imidazoles as tubulin polymerization inhibitors. Eur J Med Chem. 2021;226:113826.

12. Xu Q, Bao K, Sun M, Xu J, Wang Y, Tian H, Zuo D, Guan Q, Wu Y, Zhang W. Design, synthesis and structure-activity relationship of 3,6-diaryl-7H-[1,2,4]triazolo[3,4-b][1,3,4]thiadiazines as novel tubulin inhibitors. Sci Rep. 2017;7(1):11997.

13. Li L, Jiang S, Li X, Liu Y, Su J, Chen J. Recent advances in trimethoxyphenyl (TMP) based tubulin inhibitors targeting the colchicine binding site. Eur J Med Chem. 2018;151:482–494.

14. Eissa IH, Dahab MA, Ibrahim MK, Alsaif NA, Alanazi AZ, Eissa SI, Mehany ABM, Beauchemin AM. Design and discovery of new antiproliferative 1,2,4-triazin-3(2H)-ones as tubulin polymerization inhibitors targeting colchicine binding site. Bioorg Chem. 2021;112:104965.

15. Hagras M, El Deeb MA, Elzahabi HSA, Elkaeed EB, Mehany ABM, Eissa IH. Discovery of new quinolines as potent colchicine binding site inhibitors: design, synthesis, docking studies, and anti-proliferative evaluation. J Enzyme Inhib Med Chem. 2021;36(1):640–658.

16. Ling Y, Hao ZY, Liang D, Zhang CL, Liu YF, Wang Y. The expanding role of pyridine and dihydropyridine scaffolds in drug design. Drug Des Dev Ther. 2021;15:4289–4338.

17. Sigel E, Steinmann ME. Structure, function, and modulation of GABA(A) receptors. J Biol Chem. 2012;287(48): 40224–40231.

18. Walan A, Bader JP, Classen M, Lamers CB, Piper DW, Rutgersson K, Eriksson S. Effect of omeprazole and ranitidine on ulcer healing and relapse rates in patients with benign gastric ulcer. N Engl J Med. 1989;320(2):69–75.

19. Álvarez R, Aramburu L, Puebla P, Caballero E, González M, Vicente A, Medarde M, Peláez R. Pyridine based antitumour compounds acting at the colchicine site. Curr Med Chem. 2016;23(11):1100–1130.

20. He J, Zhang M, Tang L, Liu J, Zhong J, Wang W, Xu JP, Wang HT, Li XF, Zhou ZZ. Synthesis, biological evaluation, and molecular docking of arylpyridines as antiproliferative agent targeting tubulin. ACS Med Chem Lett. 2020;11(8): 1611–1619.

21. Ashraf M, Shaik TB, Malik MS, Syed R, Mallipeddi PL, Vardhan M, Kamal A. Design and synthesis of cis-restricted benzimidazole and benzothiazole mimics of combretastatin A-4 as antimitotic agents with apoptosis inducing ability. Bioorg Med Chem Lett. 2016;26(18):4527–4535.

22. Zheng S, Zhong Q, Mottamal M, Zhang Q, Zhang C, Lemelle E, McFerrin H, Wang G. Design, synthesis, and biological evaluation of novel pyridine-bridged analogues of combretastatin-A4 as anticancer agents. J Med Chem. 2014;57(8): 3369–3381.

23. Weiss R, Golisano T, Pale P, Mamane V. Insight into the modes of activation of pyridinium and bipyridinium salts in non-covalent organocatalysis. Adv Synth Catal. 2021;363(20): 4779–4788.

24. Yang F, Jian XE, Diao PC, Huo XS, You WW, Zhao PL. Synthesis, and biological evaluation of 3,6-diaryl-[1,2,4]triazolo[4,3-a]pyridine analogues as new potent tubulin polymerization inhibitors. Eur J Med Chem. 2020;204:112625.

25. Li G, Wang Y, Li L, Ren Y, Deng X, Liu J, Wang W, Luo M, Liu S, Chen J. Design, synthesis, and bioevaluation of pyrazolo[1,5-a]pyrimidine derivatives as tubulin polymerization inhibitors targeting the colchicine binding site with potent anticancer activities. Eur J Med Chem. 2020;202:112519.

26. Wang C, Yang S, Du J, Ni J, Wu Y, Wang J, Guan Q, Zuo D, Bao K, Wu Y, et al. Synthesis and bioevaluation of diarylpyrazoles as antiproliferative agents. Eur J Med Chem. 2019;171: 1–10.

27. Jadala C, Sathish M, Anchi P, Tokala R, Lakshmi UJ, Reddy VG, Shankaraiah N, Godugu C, Kamal A. Synthesis of combretastatin-A4 carboxamidest that mimic sulfonyl piperazines by a molecular hybridization approach: in vitro cytotoxicity evaluation and inhibition of tubulin polymerization. ChemMedChem. 2019;14(24):2052–2060.

28. Wang C, Li Y, Liu T, Wang Z, Zhang Y, Bao K, Wu Y, Guan Q, Zuo D, Zhang W. Design, synthesis and evaluation of antiproliferative and antitubulin activities of 5-methyl-4-aryl-3-(4-arylpiperazine-1-carbonyl)-4H-1,2,4-triazoles. Bioorg Chem. 2020;104:103909.

29. Kamal A, Srinivasa Reddy T, Polepalli S, Shalini N, Reddy VG, Subba Rao AV, Jain N, Shankaraiah N. Synthesis and biological evaluation of podophyllotoxin congeners as tubulin polymerization inhibitors. Bioorg Med Chem. 2014;22(19): 5466–5475.

30. Kraus Y, Glas C, Melzer B, Gao L, Heise C, Preuße M, Ahlfeld J, Bracher F, Thorn-Seshold O. Isoquinoline-based biaryls as a robust scaffold for microtubule inhibitors. Eur J Med Chem. 2020;186:111865.

31. Sana S, Reddy VG, Srinivasa Reddy T, Tokala R, Kumar R, Bhargava SK, Shankaraiah N. Cinnamide derived pyrimidine-benzimidazole hybrids as tubulin inhibitors: synthesis, in silico and cell growth inhibition studies. Bioorg Chem. 2021; 110:104765.

32. Tian C, Chen X, Zhang Z, Wang X, Liu J. Design and synthesis of (2-(phenylamino)thieno[3,2-d]pyrimidin-4-yl)(3,4,5-trimethoxyphenyl)methanone analogues as potent anti-tubulin polymerization agents. Eur J Med Chem. 2019;183:111679.

33. Sultana F, Reddy Bonam S, Reddy VG, Nayak VL, Akunuri R, Rani Routhu S, Alarifi A, Halmuthur MSK, Kamal A. Synthesis of benzo[d]imidazo[2,1-b]thiazole-chalcone conjugates as microtubule targeting and apoptosis inducing agents. Bioorg Chem. 2018;76:1–12.

34. Wang C, Li Y, Liu Z, Wang Z, Liu Z, Man S, Zhang Y, Bao K, Wu Y, Guan Q, et al. Design, synthesis and biological evaluation of 1-Aryl-5-(4-arylpiperazine-1-carbonyl)-1H-tetrazols as novel microtubule destabilizers. J Enzyme Inhib Med Chem. 2021;36(1):549–560.